Extension of Stability Radius to Neuromechanical Systems with Structured Real Perturbations

David Hajdu, John Milton and Tamas Insperger

***Abstract*—The ability of humans to maintain balance about an unstable position in a continuously changing environment attests to the robustness of their balance control mechanisms to perturbations. A mathematical tool to analyze robust stabilization of unstable equilibria is the stability radius. Based on the pseudospectra, the stability radius gives a measure to the maximum change of the system parameters without resulting loss of stability. Here we compare stability radii for a model for human frontal plane balance controlled by a delayed proportional-derivative feedback to two types of perturbations: unstructured complex and weighted structured real. It is shown that 1) narrow stance widths are more robust to parameter variation; 2) stability is maintained for larger structured real perturbations than for unstructured complex perturbations; and 3) the most robust derivative gain to weighted structured real perturbations is located near the stability boundary. It is argued that stability radii can effectively be used to compare different control concepts associated with human motor control.**

***Index Terms*—robustness, stability radii, neural engineering, time-delay systems, neurofeedback, biomechanics.**

I. Introduction

THE high morbidity and mortality associated with falls in the elderly provides a strong motivation to understand the nature of the mechanisms that maintain human balance [1], [2]. One challenge is to uncover the peculiarity of the control algorithm that is capable of stabilizing unstable equilibria in the presence of delay. However once stabilization is achieved a second challenge arises, namely, how robust is the control in the face of changes in system parameters that arise because of the effects of external perturbations and changes in posture?

The effects of external perturbations on the nervous system are most often manifested through effects on systems parameters. Periodic perturbations, e.g. parametric excitation, can stabilize an inverted pendulum [3] and prolong the time that a stick can be balanced on the fingertip [4]. Random perturbations, namely parametric noise, underlie the spontaneous fluctuations in pupil size [5] and has important roles in motor [6], [7], [8] and balance [9], [10], [11], [12] control. For balance control during quiet standing, changes in control parameters can be associated with changes in stance width [13], [14], [15].

In robust control theory two more general concepts are used to describe the effects of parameter perturbations on stability. First, the parameter perturbations can be real or complex valued [16], [17], [18]. Second, the magnitude of the effects of perturbations on system parameters may be unstructured, i.e. unrelated to the unperturbed system parameters, or may be structured or weighted structured to reflect a dependence on system parameters [19], [20], [21]. Physical interpretation of complex-valued perturbations of systems with real parameters is controversial, since the real characteristic roots can become complex without a conjugate pair. Unstructured perturbations can lead to irrelevant or non-physical effects. Consequently it is important to determine the robustness of stability for balance control to structured real perturbations.

In a seminal paper, Bingham and Ting [14] introduced the techniques of pseudospectral analysis and robust control to study the effects of unstructured complex perturbations on the control of human balance. The key concept is that of the stability radius [19], namely the magnitude of the change in some system parameters, such as the inertia or the geometric dimensions, required to destabilize the control mechanism. In [14], a model of human frontal plane balance with delayed proportional-derivative feedback [13], [22], [23] subjected to unstructured complex perturbations was analyzed. Surprisingly, it was found that the stability radius increases with decreasing stance width and, for a given stance width, the more robust gains are located in the middle of the stable region in the unperturbed parameter space.

Here we extend this approach by computing the stability radii for the same model for balance control subjected to weighted structured real perturbations. Our analysis confirms the observation that the maximum stability radius increases with decreasing stance width. However, there are two important caveats. First, the maximum perturbation required to cause instability is approximately 6-10 times larger than obtained for complex unstructured perturbations. In other words, the stability radii computed by Bingham and Ting [14] are very conservative. Second, the most robust derivative gain is located very close to the lower stability boundary. This observation is consistent with previous suggestion that feedback gains for human balance control may be tuned very close to stability boundaries [10], [24].

The outline of this paper is as follows. In Section II, we present the model for human frontal plane balance control developed by Bingham and co-workers [13]. The concepts of pseudospectra and stability radius are briefly reviewed in Section III with special attention to unstructured complex and weighted structured real perturbations. Then, in Section IV, we compare the stability radii calculated for the balance model subjected to unstructured complex perturbations and to those obtained for weighted structured real perturbations. Finally, we

D. Hajdu is with the Dept. of Applied Mechanics, Budapest University of Technology and Economics, Budapest, Hungary, e-mail: hajdu@mm.bme.hu
J. Milton is with the W. M. Keck Science Center, Claremont Colleges, Claremont, CA 91771, USA, e-mail: jmilton@jsd.claremont.edu
T. Insperger is with the Dept. of Applied Mechanics, Budapest Univ. of Tech. and Economics, Budapest, Hungary, e-mail: insperger@mm.bme.hu

discuss further applications of these techniques to the study of human balance control.

II. Dynamical Model

We investigate the mechanical model of frontal-plane balance control introduced in [13]. The corresponding four-bar linkage mechanism is shown in Fig. 1. The outer links represent the legs and the link in the middle replaces the torso. The center of masses are indicated by gray dots. The stabilizing joint torque T, which is a result of a feedback mechanism, is acting at the hips. The anthropometric data for the four-bar linkage model is given in Table I according to [13]. The two parameters of interest are the hip width W and the stance width S. Following [13], the feedback delay is set to $\tau = 150$ms.

A. Linearized equation of motion

The equation of motion can be derived using the Lagrange's equations of the second kind. According to [13], the generalized coordinate of the one-degree-of-freedom mechanism is taken to be the angle $\varphi_1(t)$. Introduce perturbation $q(t) = \varphi_1(t) - \varphi_1^*$, where φ_1^* corresponds to the upper equilibrium of the body. The linearized equation of motion can then be written as

$$\tilde{I}\,\ddot{q}(t) + \tilde{G}\,q(t) = Q(t), \tag{1}$$

where the reduced inertia $\tilde{I}$ and the gravitational term $\tilde{G}$ are calculated as

$$\tilde{I} = 2(m_{\mathrm{L}}L^2 + I_{\mathrm{L}}) + \frac{m_{\mathrm{T}}(h_{\mathrm{T}}\alpha - W\beta)^2 + I_{\mathrm{T}}\alpha^2}{W^2}, \tag{2}$$

$$\tilde{G} = -g\left(\frac{m_{\mathrm{T}}(h_{\mathrm{T}}\alpha)^2}{W^2} - \frac{(2lm_{\mathrm{L}} + Lm_{\mathrm{T}})(\alpha\beta^2 - L^2S)}{LW\beta}\right) \tag{3}$$

with

$$\alpha = S - W \quad \text{and} \quad \beta = \frac{1}{2}\sqrt{4\mathrm{L}^2 - \alpha^2}. \tag{4}$$

Since $\tilde{G} < 0$, the system is unstable when $Q(t) \equiv 0$. Assuming delayed proportional-derivative feedback mechanism, the generalized force $Q(t)$ can be written as

$$Q(t) = -C_i(k_{\mathrm{p}}q(t-\tau) + k_{\mathrm{d}}\dot{q}(t-\tau)), \tag{5}$$

where k_{p} and k_{d} are the proportional and derivative control gains, τ is the reflex delay and C_i is a constant, which depends on the choice of the feedback signal. If the hip's angular position and velocity is used as feedback signal (i.e., if the actual joint torque is $T(t) = k_{\mathrm{p}}\varphi_2(t-\tau) + k_{\mathrm{d}}\dot{\varphi}_2(t-\tau)$), then

$$C_i = C_{\mathrm{hip}} := \frac{S}{W}\frac{S-W}{W}, \tag{6}$$

where S is the stance width and W is the hip width. If the center of mass excursion is used as feedback signal, then

$$C_i = C_{\mathrm{com}} := \frac{S}{W}\frac{h_{\mathrm{T}}Lm_{\mathrm{T}}\alpha - W(Lm_{\mathrm{T}} + 2lm_{\mathrm{L}})\beta}{LW(2m_{\mathrm{L}} + m_{\mathrm{T}})}. \tag{7}$$

In [13] and [14], these two types of feedback signals were analyzed. Note that the case $C_i = C_{\mathrm{hip}}$ presents a singularity when $S = W$ since in this case $\varphi_1 = \varphi_3$ while the trunk is always vertical ($\varphi_2 = 0$). Therefore, here we rather concentrate on the control of the center of mass. There is a debate whether the center of mass position is directly controlled by the neural system or it is controlled indirectly through the body geometry [25]. Although this question has important neurological implications, from a mathematical point of view, indirect control of the center of mass for small displacements corresponds only to a reparametrization of the equations associated with direct control. The fact that many sensory organs for balance are in the head suggests that the control of the position of the head is also a possible control strategy, namely

$$C_i = C_{\mathrm{head}} := \frac{S}{W}\left(\frac{\alpha h_{\mathrm{H}}}{W} - \beta - \frac{\alpha}{W}\right), \tag{8}$$

where h_{H} indicates the distance of the head from the middle of the hip.

As in [14], it is assumed that the delay and the control gains are invariant to system changes (see also [15]) and only the parameters of the mechanical model vary. The variations

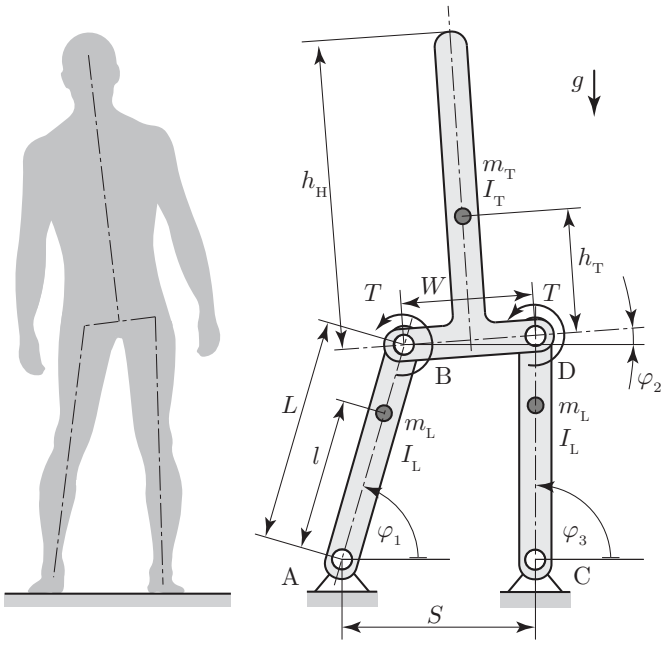

Fig. 1. The frontal-plane model of human mediolateral balance control including a four-bar linkage mechanism according to [13].

TABLE I
Anthropometric data from [13].

Description	Symbol	Value	Unit
Nominal human mass	m	70	kg
Nominal human height	h	1.8	m
Leg mass	m_{L}	$0.161m$	kg
Leg length	L	$0.53h$	m
Leg center of mass	l	$0.293h$	m
Leg inertia	I_{L}	$0.03mh^2$	kgm^2
Trunk mass	m_{T}	$0.678m$	kg
Trunk center of mass	h_{T}	$0.108h_{\mathrm{T}}$	kgm^2
Trunk inertia	I_{T}	$0.02m_{\mathrm{T}}h_{\mathrm{T}}^2$	m

in the model parameters can be represented as uncertainties in the reduced inertia $\tilde{I}$, the gravitational term $\tilde{G}$ and the configuration-dependent coefficient C_i. In order to concentrate the uncertain parameters, Eq. (1) is rearranged in the form

$$I\ddot{q}(t) + Gq(t) = -k_{\mathrm{p}}q(t-\tau) - k_{\mathrm{d}}\dot{q}(t-\tau), \tag{9}$$

where

$$I = \frac{\tilde{I}}{C_i} \quad \text{and} \quad G = \frac{\tilde{G}}{C_i}. \tag{10}$$

Now all of the uncertainties are included in the normalized parameters I and G. The equation of motion can then be written in the first-order form

$$\dot{\mathbf{x}}(t) = \mathbf{A}\mathbf{x}(t) + \mathbf{B}\mathbf{K}^{\mathrm{T}}\mathbf{x}(t-\tau) \tag{11}$$

with $\mathbf{x}(t) = (q(t),\ \dot{q}(t))^{\mathrm{T}}$ and

$$\mathbf{A} = \begin{pmatrix} 0 & 1 \\ -\frac{G}{I} & 0 \end{pmatrix},\ \mathbf{B} = \begin{pmatrix} 0 \\ \frac{1}{I} \end{pmatrix},\ \mathbf{K} = \begin{pmatrix} -k_{\mathrm{p}} \\ -k_{\mathrm{d}} \end{pmatrix}. \tag{12}$$

We are interested in the robustness of this system against changes in the parameters I and G.

III. Robust stability analysis

In [14], the robust stability of system (11) was determined using the complex stability radius associated with the perturbation of matrix $\mathbf{A}$. This corresponds to perturbation of each elements of $\mathbf{A}$ by a complex number (including the entries 0 and 1, which shall be invariant to system changes). This approach gives a conservative estimate of the actual robust stability associated with structured real perturbations. Furthermore, uncertainties of the mechanical parameters affects not only the system matrix $\mathbf{A}$ but also the input matrix $\mathbf{B}$. This effect was also neglected in [14]. In this section, the robust stability analysis is presented in case of real-valued changes of the parameters I and G. First, the ϵ-pseudospectrum is reviewed, then unstructured complex, weighted structured complex, unstructured real and weighted structured real stability radii are given step-by-step according to the literature [17], [18], [20], [21].

The ϵ-pseudospectrum σ_ϵ of a matrix $\mathbf{A}$ is defined as

$$\sigma_\epsilon := \{\lambda \in \mathbb{C} : \lambda \in \sigma(\mathbf{A} + \delta\mathbf{A}),\ \text{where } \|\delta\mathbf{A}\| < \epsilon\}, \tag{13}$$

where σ denotes the spectrum, $\|\cdot\|$ is an arbitrary matrix norm and $\delta\mathbf{A}$ is a perturbation matrix [26]. It is known, that Eq. (13) is equivalent to

$$\sigma_\epsilon := \{\lambda \in \mathbb{C} : \|\mathrm{R}(\lambda, \mathbf{A})\| > 1/\epsilon\}, \tag{14}$$

where $\mathrm{R}(\lambda, \mathbf{A}) = (\lambda\mathbf{I} - \mathbf{A})^{-1}$ denotes the corresponding resolvent operator with $\mathbf{I}$ being the identity matrix. The ϵ-pseudospectrum plays an important role in the definition of stability radius of time-delay systems.

A. Unstructured complex stability radius

Perturbations of the system matrix $\mathbf{A}$ is characterized by the perturbation matrix $\delta\mathbf{A}$. The corresponding perturbed equation reads

$$\dot{\mathbf{x}}(t) = (\mathbf{A} + \delta\mathbf{A})\mathbf{x}(t) + \mathbf{B}\mathbf{K}^{\mathrm{T}}\mathbf{x}(t-\tau). \tag{15}$$

According to the stability radii theorem (see, e.g., [17]), the unstructured complex stability radius corresponding to the complex-valued perturbation of the entire system matrix $\mathbf{A}$ reads

$$r_{\mathbb{C}}^{\mathbf{A}} = \left(\sup_{\omega \geq 0} \|(\mathrm{i}\omega\mathbf{I} - \mathbf{A} - \mathbf{B}\mathbf{K}^{\mathrm{T}}\mathrm{e}^{-\mathrm{i}\omega\tau})^{-1}\|_2 \right)^{-1}, \tag{16}$$

where $\|\cdot\|_2$ denotes the spectral norm. If the nominal system with $\delta\mathbf{A} = \mathbf{0}$ is stable, then the perturbed system with any $\delta\mathbf{A}$ satisfying the condition $\|\delta\mathbf{A}\|_2 < r_{\mathbb{C}}^{\mathbf{A}}$ is stable, too. Consequently, the robust stability boundaries for perturbations of different sizes are given by the contour curves of $r_{\mathbb{C}}^{\mathbf{A}}$.

In case of perturbations of the input matrix $\mathbf{B}$ by $\delta\mathbf{B}$, the governing equation reads

$$\dot{\mathbf{x}}(t) = \mathbf{A}\mathbf{x}(t) + (\mathbf{B} + \delta\mathbf{B})\mathbf{K}^{\mathrm{T}}\mathbf{x}(t-\tau). \tag{17}$$

The corresponding complex stability radius reads

$$r_{\mathbb{C}}^{\mathbf{B}} = \left(\sup_{\omega \geq 0} \|\mathrm{e}^{-\mathrm{i}\omega\tau}\mathbf{K}^{\mathrm{T}}(\mathrm{i}\omega\mathbf{I} - \mathbf{A} - \mathbf{B}\mathbf{K}^{\mathrm{T}}\mathrm{e}^{-\mathrm{i}\omega\tau})^{-1}\|_2 \right)^{-1}. \tag{18}$$

The unstructured complex stability radius corresponds to a complex perturbation of all the elements of the matrices $\mathbf{A}$ and $\mathbf{B}$ (even the elements 0 and 1), and is therefore a conservative estimation of the actual stability radius. A more realistic stability radius is the weighted structured stability radius, where each of the system parameters I, G are perturbed individually.

B. Weighted structured complex stability radius

The characteristic equation of (11) on the imaginary axis can be written in the form

$$\begin{aligned} D(\omega) &= \det(\mathrm{i}\omega\mathbf{I} - \mathbf{A} - \mathbf{B}\mathbf{K}^{\mathrm{T}}\mathrm{e}^{-\mathrm{i}\omega\tau}) \\ &= I(\mathrm{i}\omega)^2 + G + k_{\mathrm{p}}\mathrm{e}^{-\mathrm{i}\omega\tau} + k_{\mathrm{d}}\mathrm{i}\omega\mathrm{e}^{-\mathrm{i}\omega\tau}. \end{aligned} \tag{19}$$

In case of weighted perturbations of the system parameters as $I + \delta I$ and $G + \delta G$, the perturbation matrix should be introduced

$$\mathbf{\Delta} = \begin{pmatrix} w_I\,\delta I \\ w_G\,\delta G \end{pmatrix}, \tag{20}$$

where w_I and w_G are the weights of the perturbations with respect to the nominal inertia I and the nominal gravitational term G, respectively. If $|\delta I| < \varepsilon_I|I|$ and $|\delta G| < \varepsilon_G|G|$, where ε_I and ε_G are the radii of uncertainties, then the corresponding weights are

$$w_I = \frac{1}{\varepsilon_I I}, \quad w_G = \frac{1}{\varepsilon_G G}. \tag{21}$$

For instance, if I is perturbed by maximum 2%, then $w_I = (0.02I)^{-1}$. If $w_I \to \infty$ or $w_G \to \infty$ then no perturbation

on I or on G is allowed [20]. This formalism allows the perturbations satisfying

$$(\|\mathbf{\Delta}\|_2)^2 = \left|\frac{\delta I}{\varepsilon_I I}\right|^2 + \left|\frac{\delta G}{\varepsilon_G G}\right|^2 \leq 1. \tag{22}$$

Thus, the allowed perturbations lie within an ellipse of main axes $\varepsilon_I I$ and $\varepsilon_G G$ in the plane $(\delta I, \delta G)$.

Following [20], the complex stability radius corresponding to the perturbation matrix $\mathbf{\Delta}$ can be calculated as

$$r_{\mathbb{C}}^{\mathbf{\Delta}} = \frac{1}{\sup_{\omega\geq 0} \|D(\omega)^{-1}\mathbf{w}(\omega)\|_2}, \tag{23}$$

where $\mathbf{w}(\omega)$ is the complex weight function

$$\mathbf{w}(\omega) = \begin{pmatrix} \frac{(\mathrm{i}\omega)^2}{w_I} & \frac{1}{w_G} \end{pmatrix}. \tag{24}$$

If the nominal system is stable and $r_{\mathbb{C}}^{\mathbf{\Delta}} < 1$, then the system is robustly stable for any perturbations satisfying (22). Consequently the robust stability boundary associated with the uncertainty radii ε_I and ε_G is given by the contour curve $r_{\mathbb{C}}^{\mathbf{\Delta}} = 1$. Contour curves $r_{\mathbb{C}}^{\mathbf{\Delta}} = z$ with any $z \in \mathbb{R}^+$ give the robust stability boundaries associated with the uncertainty radii $z\varepsilon_I$ and $z\varepsilon_G$.

C. Unstructured real stability radius

If only real entries of the perturbation matrix $\delta\mathbf{A}$ in (15) are allowed, then the corresponding real stability radius can be calculated following [17] and [18] as

$$r_{\mathbb{R}}^{\mathbf{A}} = \frac{1}{\sup_{\omega\geq 0} \mu_{\mathbb{R}}(\mathbf{W}(\omega))}, \tag{25}$$

where

$$\mu_{\mathbb{R}}(\mathbf{W}(\omega)) = \inf_{\gamma\in(0,1]} \sigma_2 \begin{pmatrix} \mathfrak{Re}\mathbf{W} & -\gamma\mathfrak{Im}\mathbf{W} \\ \gamma^{-1}\mathfrak{Im}\mathbf{W} & \mathfrak{Re}\mathbf{W} \end{pmatrix} \tag{26}$$

and

$$\mathbf{W}(\omega) = (\mathrm{i}\omega\mathbf{I} - \mathbf{A} - \mathbf{B}\mathbf{K}^{\mathrm{T}}\mathrm{e}^{-\mathrm{i}\omega\tau})^{-1}. \tag{27}$$

Here σ_2 denotes the second largest singular value.

Similarly, in case of real-valued perturbation of the input matrix $\mathbf{B}$, the real stability radius reads

$$r_{\mathbb{R}}^{\mathbf{B}} = \frac{1}{\sup_{\omega\geq 0} \mu_{\mathbb{R}}(\mathbf{W}(\omega))}, \tag{28}$$

with (26) and

$$\mathbf{W}(\omega) = \mathrm{e}^{-\mathrm{i}\omega\tau}\mathbf{K}^{\mathrm{T}}(\mathrm{i}\omega\mathbf{I} - \mathbf{A} - \mathbf{B}\mathbf{K}^{\mathrm{T}}\mathrm{e}^{-\mathrm{i}\omega\tau})^{-1}. \tag{29}$$

D. Weighted structured real stability radius

Weighted structured real stability radius is a straightforward combination of unstructured real [17], [18] and weighted structured complex [20], [21] stability radii and can be calculated as

$$r_{\mathbb{R}}^{\mathbf{\Delta}} = \frac{1}{\sup_{\omega\geq 0} \mu_{\mathbb{R}}(\mathbf{W}(\omega))}, \tag{30}$$

where

$$\mu_{\mathbb{R}}(\mathbf{W}(\omega)) = \inf_{\gamma\in(0,1]} \sigma_2 \begin{pmatrix} \mathfrak{Re}\mathbf{W} & -\gamma\mathfrak{Im}\mathbf{W} \\ \gamma^{-1}\mathfrak{Im}\mathbf{W} & \mathfrak{Re}\mathbf{W} \end{pmatrix} \tag{31}$$

and

$$\mathbf{W}(\omega) = D(\omega)^{-1}\mathbf{w}(\omega). \tag{32}$$

Here, $\mathbf{\Delta}$ is defined as in (20). Similarly to the previous cases, the robust stability boundaries associated with the uncertainty radii ε_I and ε_G is given by the contour curve $r_{\mathbb{R}}^{\mathbf{\Delta}} = 1$, while the contour curves $r_{\mathbb{R}}^{\mathbf{\Delta}} = z$, $z \in \mathbb{R}^+$ give the boundaries associated with the uncertainty radii $z\varepsilon_I$ and $z\varepsilon_G$.

IV. Results

Stability boundaries of the nominal system (without perturbation) in terms of the delayed feedback gains can be found in [13]. Robust stability boundaries in case of complex unstructured perturbation of the system matrix $\mathbf{A}$ were provided in [14]. Here, robust stability analysis is presented for real-valued perturbation on the system parameters I and G. The stable regions of the nominal system in the parameter plane $(k_{\mathrm{p}}, k_{\mathrm{d}})$ were determined numerically using the semi-discretization method [27]. Stability radii and the robust stability boundaries are determined only in the stable regions.

In order to be able to compare the unstructured complex stability radius with the weighted structured real one, we introduce the relative stability radii. For complex perturbation, we use the ratio of the norm of the perturbation and the norm of the state matrix:

$$\tilde{r}_{\mathbb{C}}^{\mathbf{A}} := \frac{r_{\mathbb{C}}^{\mathbf{A}}}{\|\mathbf{A}\|_2}. \tag{33}$$

This number gives the relative complex perturbation that is allowed on the system matrix $\mathbf{A}$ without losing stability. For weighted structured real perturbation, we set the uncertainty radii to $\varepsilon_I = 1$ and $\varepsilon_G = 1$ and introduce the relative stability radius as

$$\tilde{r}_{\mathbb{R}}^{\mathbf{\Delta}} := r_{\mathbb{R}}^{\mathbf{\Delta}}\Big|_{\substack{\varepsilon_I=1 \\ \varepsilon_G=1}}. \tag{34}$$

This number gives the relative real perturbation that is allowed on the inertia I and the gravitational term G without loosing stability. Now, the relative stability radii $\tilde{r}_{\mathbb{C}}^{\mathbf{A}}$ and $\tilde{r}_{\mathbb{R}}^{\mathbf{\Delta}}$ can directly be compared.

Figure 2 compares the robust stability boundaries and the pseudospectra calculated using complex unstructured and real weighted structured perturbations. Panel a) in Fig. 2 shows the robust stability boundaries for complex unstructured perturbations of the system matrix $\mathbf{A}$ using the same concept as in [14]. The equation under analysis is given in the first order form (11) and the robust stability boundaries are determined using the complex stability radius given by (16). Different contour curves associated with relative stability radii $\tilde{r}_{\mathbb{C}}^{\mathbf{A}} = 0, 0.02, \ldots, 0.08$ are presented. These contour curves corresponds to $0, 2, \ldots, 8\%$ complex perturbation of the system matrix $\mathbf{A}$.

Panel b) in Fig. 2 illustrates the pseudospectrum associated with the control gains $k_{\mathrm{p}} = 1140$ and $k_{\mathrm{d}} = 290$. This point is indicated by point A in panel a). The three rightmost characteristic roots are indicated by black dots and their pseudospectra associated with different perturbation levels are indicated by thin lines. The relative complex stability radius

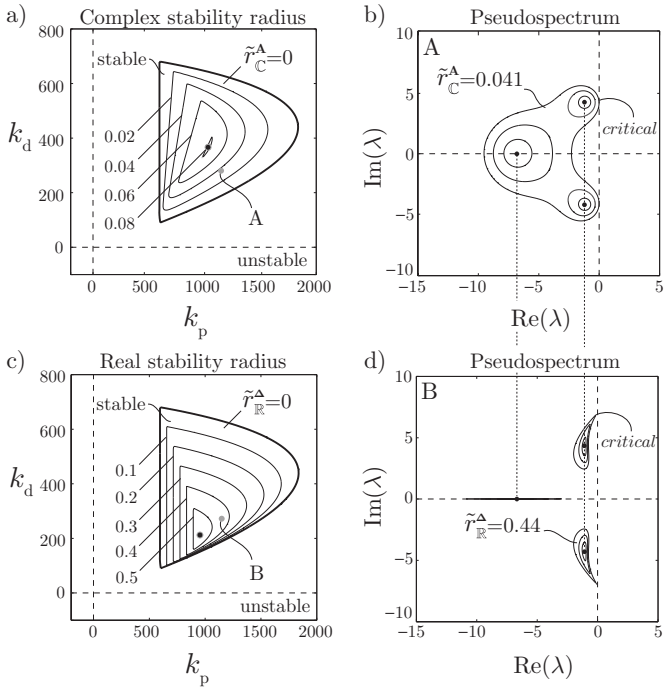

Fig. 2. Stability chart and corresponding pseudospectra with stance width ratio $S/W = 1.2$: a) complex stability radii; b) complex pseudospectra at parameter point A; c) real stability radii; d) real pseudospectra at parameter point B.

at this parameter point is $\tilde{r}_{\mathbb{C}}^{\mathbf{A}} = 0.041$, i.e., the corresponding pseudospectrum just touches the imaginary axis. This indicates that there exist a complex perturbation $\delta\mathbf{A}$ with $\|\delta\mathbf{A}\|_2/\|\mathbf{A}\|_2 = 0.041$ such that the perturbed system loses asymptotic stability. Thus, a 4.1% complex perturbation of $\mathbf{A}$ can already destabilize the system.

Panel c) in Fig. 2 shows the robust stability boundaries obtained by the weighted structured real stability radius according to (30) with $\varepsilon_I = 1$ and $\varepsilon_G = 1$. Different contour curves indicate different relative weighted structured real stability radii $\tilde{r}_{\mathbb{R}}^{\mathbf{\Delta}}$. For instance, the contour curves $\tilde{r}_{\mathbb{R}}^{\mathbf{\Delta}} = 0.1$ indicates the robust stability boundaries corresponding to maximum 10% perturbation of the inertia I and maximum 10% perturbation of the gravitational term G.

Panel d) in Fig. 2 shows the pseudospectra corresponding to the same control gains as in panel b). This point is also indicated by point B in panel c). It can be seen that the change of the three rightmost characteristic roots for real perturbations is qualitatively different from that of the complex perturbations: the real characteristic multipliers of the nominal system remain real and moves on the real axis as the perturbation changes. The wandering of the complex pair of eigenvalues is also different: they sharply drifts to the imaginary axis in a specific direction. The relative real stability radius at this parameter point is $\tilde{r}_{\mathbb{R}}^{\mathbf{\Delta}} = 0.44$. This means that the system can loose stability if the real-valued perturbations satisfy

$$\left(\frac{\delta I}{0.44I}\right)^2 + \left(\frac{\delta G}{0.44G}\right)^2 \geq 1. \tag{35}$$

In other words, larger than 44% perturbation on the inertia I

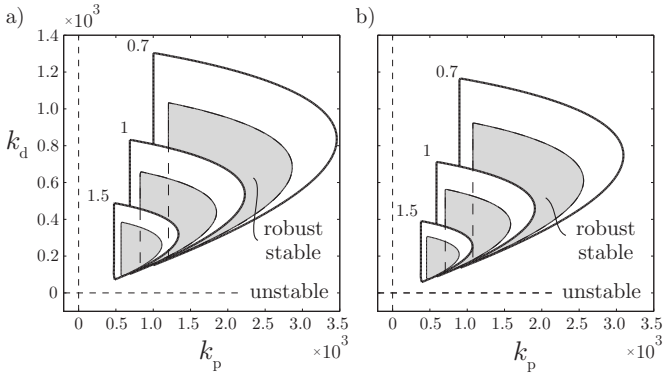

Fig. 3. Stable (white) and robustly stable (gray) domains for stance width ratios $S/W = 0.7, 1, 1.5$ for different feedback concepts: a) position feedback of center of mass excursion; b) position feedback of head excursion. The uncertainties of both the inertia and gravitational terms are 20%.

or on the gravitational term G can destabilize the system. This numerical example demonstrates that the complex stability radius gives a strongly conservative estimate of the relative stability radius. 4.1% relative complex perturbation on the system matrix $\mathbf{A}$ may already destabilize the system, while the size of the relative real perturbation on I and G, which gives an unstable system, is 44%. The maximum relative stability radii in the robust stability diagrams show a similar tendency: $\tilde{r}_{\mathbb{C}}^{\mathbf{A}} = 0.0814$ while $\tilde{r}_{\mathbb{R}}^{\mathbf{\Delta}} = 0.5801$ (both points are indicated by dots in panels a) and c) of Fig. 2).

Figure 3 shows the effect of the use of different feedback signals. Panel a) shows the case when the position and the velocity of the center of mass is applied as feedback signal according to [13], [14] ($C_i = C_{\mathrm{com}}$). Panel b) presents the case when the feedback signal is the position and the velocity of the head ($C_i = C_{\mathrm{head}}$). The uncertainty radii for both cases are $\varepsilon_I = 0.2$ and $\varepsilon_G = 0.2$, i.e., the maximum perturbations are 20% for both parameters. Although the robust stability boundaries are different for the two feedback concepts, they are similar in topology, namely, there is no choice of $(k_{\mathrm{p}}, k_{\mathrm{d}})$, which can robustly stabilize the system for stance width ratios S/W ranging from 0.7 to 1.5. This observation suggests that the nervous system might tune control gains to accommodate different S/W configurations.

Figure 4 shows the change of the robust stability boundaries under different size of perturbations. The panels can be considered projections of the four-dimensional robust stability diagram in the parameter space $(k_{\mathrm{p}}, k_{\mathrm{d}}, \varepsilon_I, \varepsilon_G)$. The uncertainty radius ε_I for the inertia is kept constant in each row, while each column represents constant uncertainty radius ε_G for the gravitational term. For instance, the case $\varepsilon_I = 20\%$ and $\varepsilon_G = 40\%$ corresponds to perturbations which lie within the ellipse in the plane $(\delta I, \delta G)$ defined by (22) with main axes $0.2I$ and $0.4G$.

Stable regions for delayed feedback controllers are typically bounded by a straight vertical line representing static loss of stability and a curved boundary representing dynamic loss of stability [28], [29]. It can be observed that the uncertainty of the inertia shifts the static stability boundary to the right, but does not affect significantly the dynamic stability boundary.

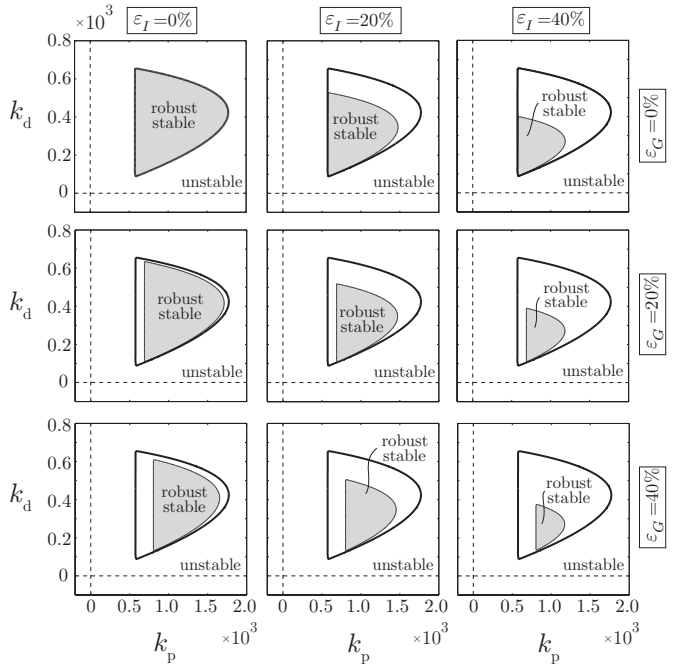

Fig. 4. Robust stability boundaries for stance width ratio $S/W = 1.2$ and for different perturbations on the inertia and the gravitational term.

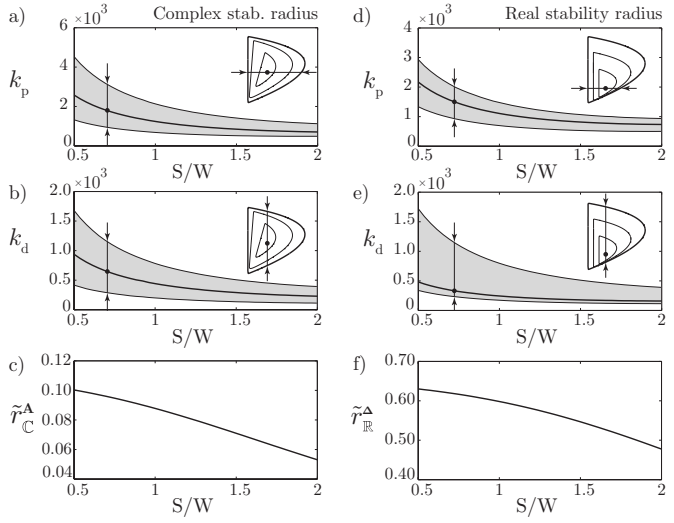

Fig. 5. Stabilizing feedback gains (gray shading in panels a,b,d,e), gains associated with maximum relative stability radii (solid line in panels a,b,d,e) and maximum relative stability radii (solid line in panels c, f). Panels a,b,c): unstructured complex stability radius according to [14]; panels d,e,f): weighted structured real stability radius.

The uncertainty in the gravitational term shifts drastically the dynamic stability boundary, but does not affect the static stability boundary. In case of the presented parameter combinations and stance widths, robust stability boundaries are more sensitive to uncertainties in the inertia than in the gravitational term.

Figure 5 shows the stabilizing feedback gains and the maximum relative stability radii for different stance width ratios. In panels a), b) and d), e), the stabilizing feedback gains are indicated by gray shading, the gains associated with the maximum relative stability radii are marked by solid lines. Panels c) and f) presents the maximum relative stability radii as function of the stance width ratio S/W. Panels a), b) and c) shows the results obtained by unstructured complex stability radius according to [14], while panels d), e) and f) correspond to the weighted structured real stability radius. For both types of perturbations the largest stability radii are associated with narrow stance widths.

There are two main differences between the complex and the real stability radii shown in panels c) and f). First, the maximum relative complex perturbation of the system matrix $\mathbf{A}$ without loosing stability is less than 10%, while this ratio for the real perturbation of the inertia and the gravitational term ranges between 48–63$\%$. Thus, the allowed real perturbation on the actual mechanical parameters is much larger than the complex one. Second, the most robust derivative gain (k_d) is located close to the lower stability boundary for the real perturbation, while it is about in the middle of the stable region for the complex perturbation. Note that the actual feedback gains fitted to human response to perturbation are in the lower left corner of the stable region [13], which corresponds to the most robust control gains obtained by the real stability radius.

Figure 6 shows simulations of the model at narrow ($S/W = 0.5$) and wide ($S/W = 2$) stance widths using the feedback gains associated with complex stability radius $r^{\mathbf{A}}_{\mathbb{C}} = 0.6$. The initial conditions for the simulations were $q(0) = 0$ and $\dot{q}(0) = 0.1$ rad/s and Matlab dde23 solver was used to determine time histories. These plots confirm the results by [14]: trajectories of the center of mass are similar for different stances while the restoring torque is significantly larger for narrow stance. The corresponding relative complex stability radii are $\tilde{r}^{\mathbf{A}}_{\mathbb{C}} = 0.074$ and 0.045, i.e., 7.4% and 4.5% complex perturbations are allowed on the system matrix $\mathbf{A}$. The relative real stability radii ($\tilde{r}^{\mathbf{\Delta}}_{\mathbb{R}} = 0.341$ and 0.275) show that these perturbations actually correspond to significantly larger perturbations on the real system parameters: 34.1% and 27.5% perturbations are allowed on the inertia and the gravitational term. It can be observed that, for these parameters, the center-of-mass trajectories are similar to the response of a critically damped system in agreement with [14].

V. Discussion

The calculation of stability radii can be used to assess the effects of parametric perturbations on the dynamics of a model for balance control with delayed proportional-derivative feedback. In other words, the control gains that are essential for the maintenance of balance are the ones associated with the largest stability radius. In a previous study [14], it was shown that the largest stability radii in response to unstructured complex perturbations occur for narrow stance widths. Here we confirmed that this is also true for more realistic perturbations and, in particular, those that take the form of weighted structured real perturbations. However, there are two quantitative differences between the effects of complex and real perturbations. First, the stability radii in response to weighted structured real perturbations are 6-10 times larger than observed for unstructured complex perturbations. Second,

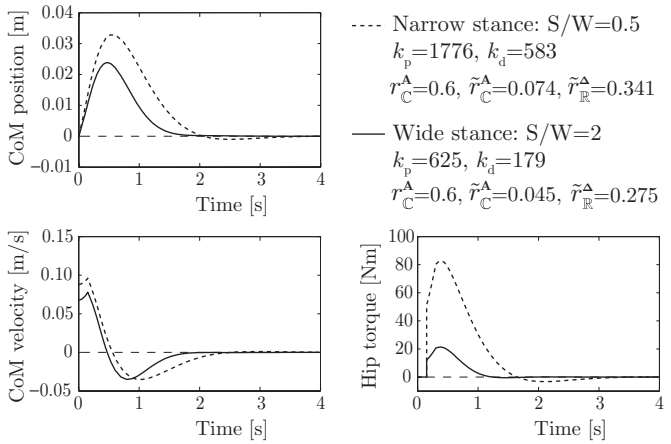

Fig. 6. Center-of-mass trajectories for different stance widths obtained by time-domain simulations using feedback gains associated with $r^{\mathbf{A}}_{\mathbb{C}} = 0.6$.

the most robust derivative gains are located closer to the stability boundary when the parameter perturbations are real valued. This latter observation is consistent with previous suggestion that feedback gains for human balance control may be tuned very close to stability boundaries in order to minimize energy requirements for maintaining balance [10], [24].

Most individuals experience greater instability when standing with a narrow stance and are typically most comfortable when $S/W \approx 1$. Thus the observation that the stability radius is largest for a narrow stance seems counterintuitive. As explained in [13], the lack of robustness at wide stance is due to the reduction in rotational inertia, while the destabilizing gravitational moment remains nearly constant, which results in an increased leverage of the muscle torque and hence a larger sensitivity to parameter perturbations. It should also be noted that the feeling of larger instability for a narrow stance is not related to the robustness against parameter perturbations, but rather robustness against perturbations in the state variables, which is associated with the basin of attraction of the equilibrium position. For example, an important requirement for the maintenance of balance during quiet standing is that the center of mass must stay within the base of support located beneath and between the soles of the feet. In mathematical terms the base of support is approximately the basin of attraction for the upright position [30]. A much studied example of the effect of perturbations in the state variables on standing balance is the ankle-hip-step strategy adopted by subjects in response to increasingly large perturbations [31], [32], [33], [34]. Presumably the unsteadiness felt by individuals standing with narrow stance widths reflect the role of other corrective mechanisms which are activated as the edge of the basin of attraction is approached [35].

Our analysis shows that the control preserves stability even for $\approx 50\%$ perturbations of the inertia. This is in some sense in agreement with the results of [36], where the effect of adding weight and inertia on balance was analyzed during quiet standing. They separated the effect of added inertia and added weight and showed that adding inertia by itself had no effect on balance while adding weight by itself had a slight negative effect on balance. It should be emphasized that in this paper we analyzed temporary perturbations of the inertia and the gravitational term, which is not equivalent to permanent change of these parameters, where the neuromuscular control gains are already adjusted. For instance, it is known that obese persons have a higher risk of falling than lightweight individuals [37]. Overweight can hardly be considered as a temporary perturbation of the inertia since individuals can accommodate their neural control gains continuously according to their actual weight. In [38], a proportional stabilizing force (an added stiffness) was applied at the hip while standing, which is equivalent to a permanent perturbation of the gravitational term. It was shown that subjects adjusted their control gains to compensate for the change in the stiffness parameter.

Previous studies have emphasized that balance control mechanisms are benefited by tuning the parameters near, or even on stability boundaries [10], [24]. It is more efficient to initiate quick movements from an unstable position than from a stable one and the energy demands for such control are relatively small. In addition, dynamical systems tuned towards the edge of stability can exhibit a variety of complex behaviors, collectively referred to as critical phenomena [39], which may provide mechanisms for self-regulated balance, e.g. on-off intermittency [10].

Many types of control mechanism have been postulated for the stabilization of unstable positions including proportional-derivative-acceleration feedback [40], [41], [42], intermittent predictive control [43], [44], intermittent activation of feedback control [45], [46], [47], predictor feedback [48], [49] and act-and-wait control [50]. Moreover, the effects of perturbations are important for other tasks related to human balance control during motion [51], such as stick balancing [10], [4], balance control during postural sway [52], [46], maintaining a constant force in an unstable environment [53] or balancing on tightropes and slacklines [54]. Since all of these tasks are impacted by parametric perturbations we anticipate that techniques, such as those related to the stability radius, will become increasingly important for identifying robust mechanisms for neural control.

ACKNOWLEDGMENT

The authors acknowledge useful discussions with Robert Peterka. This research project was partially supported by the Hungarian National Science Foundation under grant OTKAK105433 (DH, TI) and the William R. Kenan, Jr Charitable Trust (JM).

REFERENCES

[1] S. G. Leveille, D. P. Kiel, R. N. Jones, A. Roman, M. T. Hannan, F. A. Sorond, H. G. Kang, E. J. Samelson, M. Gagnon, M. Freeman, and L. A. Lipsitz, "The MOBILIZE Boston Study: Design and methods of a prospective cohort study of novel risk factors for falls in an older population," *BMC Geriatrics*, vol. 8, p. 16, 2008.

[2] F. Moss and J. Milton, "Balancing the unbalanced," *Nature*, vol. 425, pp. 911–912, 2003.

[3] T. Insperger, "Stick balancing with reflex delay in case of parametric forcing," *Commun. Nonlinear Sci.*, vol. 16, pp. 2160–2168, 2011.

[4] J. G. Milton, T. Ohira, J. L. Cabrera, R. M. Fraiser, J. B. Gyorffy, F. K. Ruiz, M. A. Strauss, E. C. Balch, P. J. Marin, and J. L. Alexander, "Balancing with vibration: A prelude for "drift and act" balance control," *PLoS ONE*, vol. 4, p. e7427, 2009.

[5] L. Stark, F. W. Campbell, and J. Atwood, "Pupil unrest: An example of noise in a biological servomechanism," *Nature*, vol. 182, pp. 857–858, 1958.

[6] F. S. Chance, L. F. Abbott, and A. D. Reyes, "Gain modulation from background synaptic input," *Neuron*, vol. 35, pp. 773–782, 2002.

[7] C. M. Harris and D. M. Wolpert, "Signal-dependent noise determines motor planning," *Nature*, vol. 394, 780-784.

[8] V. K. Jirsa, P. Fink, P. Foo, and J. A. S. Kelso, "Parametric stabilization of biological coordination: a theoretical model," *J. Biol. Phys.*, vol. 26, 2000.

[9] J. L. Bogdanoff and S. J. Citron, "Experiments with an inverted pendulum subject to random parametric excitation," *J. Acoust. Soc. Am.*, vol. 38, pp. 447–452, 1965.

[10] J. L. Cabrera and J. G. Milton, "On-off intermittency in a human balancing task," *Phys. Rev. Lett.*, vol. 89, 2002, 158702.

[11] J. L. Cabrera, R. Bormann, C. Eurich, T. Ohira, and J. Milton, "State-dependent noise and human balance control," *Fluct. Noise Lett.*, vol. 4, pp. L107–L117, 2004.

[12] A. A. Priplata, J. B. Niemi, J. Harry, L. A. Lipshitz, and J. Collins, "Vibratory insoles and balance control is elderly people," *Lancet*, vol. 362, pp. 1123–1124, 2003.

[13] J. T. Bingham, J. T. Choi, and L. H. Ting, "Stability in a frontal plane model of balance requires coupled changes to postural configuration and neural feedback control," *J. Neurophysiol.*, vol. 106, pp. 437–448, 2011.

[14] J. T. Bingham and L. H. Ting, "Stability radius as a method for comparing the dynamics of neuromechanical systems," *IEEE Trans. Neural. Syst. Rehab. Eng.*, vol. 21, no. 5, pp. 840–848, 2013.

[15] S. M. Henry, J. Fung, and F. B. Horak, "Effect of stance width on multidirectional postural responses," *J. Neurophysiol.*, vol. 85, no. 2, pp. 559–570, 2001.

[16] L. Qiu, B. Bernhardsson, A. Rantzer, E. J. Davison, P. M. Young, and J. C. Doyle, "A formula for computation of the real stability radius," *Automatica*, vol. 31, no. 6, pp. 879–890, 1995.

[17] W. Michiels and D. Roose, "An eigenvalue based approach for the robust stabilization of linear time-delay systems," *Int. J. Control*, vol. 76, no. 7, pp. 678–686, 2003.

[18] G. Hu and E. J. Davison, "Real stability radii of linear time-invariant time-delay systems," *Syst. Control Lett.*, vol. 50, pp. 209–219, 2003.

[19] D. Hinrichsen and A. J. Pritchard, "Stability radius for structured perturbations and the algebraic Riccati eauation," *Syst. Control Lett.*, vol. 8, pp. 105–113, 1986.

[20] W. Michiels, K. Green, T. Wagenknecht, and S.-I. Niculescu, "Pseudospectra and stability radii for analytic matrix functions with application to time-delay systems," *Linear Algebra Appl.*, vol. 418, pp. 315–335, 2006.

[21] T. Wagenknecht, W. Michiels, and K. Green, "Structured pseudospectra for nonlinear eigenvalue problems," *J. Comput. Appl. Math.*, vol. 212, pp. 245–259, 2008.

[22] A. D. Goodworth and R. J. Peterka, "Influence of stance width on frontal plane postural dynamics and coordination in human balance control," *J. Neurophysiol.*, vol. 104, pp. 1103–1118, 2010.

[23] ——, "Sensorimotor integration for multisegmental frontal plane balance control in humans," *J. Neurophysiol.*, vol. 107, pp. 12–28, 2012.

[24] L. Moreau and E. D. Sontag, "Balancing at the border of stability," *Phys. Rev. E*, vol. 68, p. 020901, 2003.

[25] J. Massion and M. H. Woollacott, "Posture and equilibrium," in *Clinical Disorders of Balance, Posture and Gait*, A. M. Bronsteing, T. Brandt, and M. Woollacott, Eds. New York: Oxford University Press, 1996, pp. 1–18.

[26] L. N. Trefethen and M. Embree, *Spectra and Pseudospectra*. Princeton Univ. Press, 2005.

[27] T. Insperger and G. Stepan, *Semi-discretization for time-delay systems*. New York: Springer, 2011, vol. 178.

[28] G. Stepan, *Retarded dynamical systems*. Harlow: Longman, 1989.

[29] ——, "Delay effects in the human sensory system during balancing," *Phil. T. R. Soc. A*, vol. 367, pp. 1195–1212, 2009.

[30] M. S. Zakynthinaki, J. R. Stirling, C. A. C. Martinez, A. L. D. de Durana, M. S. Quintana, G. R. Romo, and J. S. Molinuevo, "Modeling the basin of attraction as a two-dimensional manifold from experimental data: applications to balance in humans," *Chaos*, vol. 20, p. 013119, 2010.

[31] F. B. Horak and L. M. Nashner, "Central programming of postural movements: adaptation to altered support-surface configurations," *J. Neurophysiol.*, vol. 55, no. 6, pp. 1369–1381, 1986.

[32] A. Shumway-Cook and M. H. Woollacott, *Motor control: Theory and practical appications, second edition*. Lippincott Williams & Wilkins.

[33] J. L. Cabrera and J. G. Milton, "Stick balancing, falls and Dragon-Kings," *Eur. Phys. J.-Spec. Top.*, vol. 205, pp. 231–241, 2012.

[34] T. D. J. Welch and L. H. Ting, "Mechanisms of motor adaptation in reactive balance control," *PLoS ONE*, vol. 9, no. 5, 2014, e96440.

[35] L. H. Ting and K. W. van Antwerp and J. E. Scrivens and J. L. McKay and T. D. J. Welch and J. T. Bingham and S. P. DeWeerth, "Neuromechanical tuning of nonlinear postural control dynamics," *CHAOS*, vol. 19, 2009, 026111.

[36] K. E. Costello, S. L. Matrangola, and M. L. Madigan, "Independent effects of adding weight and inertia on balance during quiet standing," *Biomedical Engineering Online*, vol. 11, 2012, 20.

[37] P. Corbeil, M. Simoneau, D. Rancourt, A. Tremblay, and N. Teasdale, "Increased risk for falling associated with obesity: mathematical modeling of postural control," *IEEE Trans. Neural. Syst. Rehab. Eng.*, vol. 9, pp. 126–136, 2001.

[38] D. Engelhart, A. C. Schouten, R. G. Aarts, and H. van der Kooij, "Assessment of multi-joint coordination and adaptation in standing balance: a novel device and system identification technique," *IEEE Trans. Neural. Syst. Rehab. Eng.*, vol. 23, no. 6, pp. 973–982, 2015.

[39] W. Horsthemke and R. Lefever, *Noise-induced transitions: Theory and applications in Physics, Chemistry and Biology*. Berlin: Springer, 1984.

[40] D. B. Lockhart and L. H. Ting, "Optimal feedback transformations for balance," *Nature Neuroscience*, vol. 10, pp. 1329–1336, 2007.

[41] T. D. J. Welch and L. H. Ting, "A feedback model explains the differential scaling of human postural responses to perturbation acceleration and velocity," *J. Neurophysiol.*, vol. 101, pp. 3294–3309, 2009.

[42] T. Insperger, J. Milton, and G. Stepan, "Acceleration feedback improves balancing against reflex delay," *J. R. Soc. Interface*, vol. 10, no. 79, 2013, 20120763.

[43] P. Gawthrop, I. Loram, M. Lakie, and H. Gollee, "Intermittent control: a computational theory of human control," *Biol. Cybern.*, vol. 104, pp. 31–51, 2011.

[44] ——, "Intermittent control models of human standing: similarities and differences," *Biol. Cybern.*, vol. 108, pp. 159–168, 2014.

[45] A. Bottaro, Y. Yasutake, T. Nomura, M. Casadio, and P. Morasso, "Bounded stability of the quiet standing posture: An intermittent control model," *Hum. Movement Sci.*, vol. 27, pp. 473–495, 2008.

[46] Y. Asai, Y. Tasaka, K. Nomura, T. Nomura, M. Casidio, and P. Morasso, "A model of postural control in quiet standing: Robust compensation of delay–induced instability using intermittent activation of feedback control," *PLoS ONE*, vol. 4, p. e6169, 2009.

[47] Y. Suzuki, T. Nomura, M. Casadio, and P. Morasso, "Intermittent control with ankle, hip, and mixed strategies during quiet standing: A theoretical proposal based on a double inverted pendulum model," *J. Theor. Biol.*, vol. 310, pp. 55–79, 2012.

[48] B. Mehta and S. Schaal, "Forward models in visuomotor control," *J. Neurophysiol.*, vol. 88, pp. 942–953, 2002.

[49] T. Insperger and J. Milton, "Sensory uncertainty and stick balancing at the fingertip," *Biol. Cybern.*, vol. 108, pp. 85–101, 2014.

[50] T. Insperger, "Act and wait concept for time-continuous control systems with feedback delay," *IEEE T. Contr. Syst. T.*, vol. 14, pp. 974–977, 2006.

[51] F. J. Valero-Cuevas, H. Hoffmann, M. U. Kurse, J. J. Kutch, and E. A. Theodorou, "Computational models for neuromuscular function," *IEEE Rev. Biomed. Eng.*, vol. 2, pp. 110–135, 2009.

[52] I. D. Loram, C. N. Maganaris, and M. Lakie, "Human postural sway results from frequent, ballistic bias impulses by soleus and gastrocnemius," *J. Physiol.*, vol. 564.1, pp. 295–311, 2005.

[53] F. J. Valero-Cuevas, N. Smaby, M. Venkadesan, M. Peterson, and T. Wright, "The strength-dexterity test as a measure of dynamic pinch performance," *J. Biomech.*, vol. 36, pp. 265–270, 2003.

[54] P. Paoletti and L. Mahadevan, "Balancing on tightropes and slacklines," *J. R. Soc. Interface*, vol. 9, no. 74, pp. 2097–2108, 2012.

David Hajdu was born in Budapest, Hungary in 1990. He received his BSc and MSc degrees in mechatronics engineering and in mechanical engineering modeling from the Budapest University of Technology and Economics (BME) in 2013 and 2015, respectively. He is currently a PhD student at the Department of Applied Mechanics, BME.

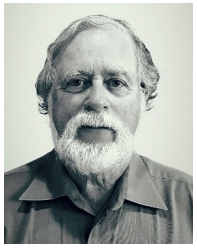

John Milton was born in Halifax, Nova Scotia, Canada in 1950. He received his BSc in biology, PhD in physical chemistry and MDCM from McGill University, Quebec, Canada in 1971, 1975 and 1982, respectively. He did his internship in internal medicine at the Royal Victoria Hospital, Montreal in 1983 and completed his neurology residency and fellowship at the Montreal Neurological Institute in 1986 and 1987, respectively.

Tamas Insperger was born in Hódmezővásárhely, Hungary in 1976. He received his MSc and PhD degrees in mechanical engineering from the Budapest University of Technology and Economics (BME) in 1999 and 2002, respectively. He is currently an associate professor at the Department of Applied Mechanics, BME.